Photonics and Nanostructures – Fundamentals and Applications 26 (2017) 1–7

Contents lists available at ScienceDirect

Photonics and Nanostructures – Fundamentals and Applications

journal homepage: www.elsevier.com/locate/photonics

Theoretical designs for novel photonic crystal nanocavities with Si (111) interfaces

Alyssa Prasmusinto, Moïse Sotto, Abdelrahman Zaher Al-Attili, Kapil Debnath, Shinichi Saito*

Nanoelectronics Nanotechnology Research Group Electronics Computer Science, Zepler Institute, Faculty of Physical Sciences Engineering, University of Southampton, SO17 1BJ, United Kingdom

ARTICLE INFO

Article history:
Received 1 November 2016
Received in revised form 7 December 2016
Accepted 13 February 2017
Available online 10 May 2017

Keywords:
Etching
Nanofabrication
Photonic crystals
Silicon-on-insulator

ABSTRACT

We designed a series of photonic crystal (PhC) nanocavities using atomically flat silicon (111) interfaces and examined the impacts of the surfaces on the optical confinement. The nanocavities were simulated using the 3D finite-difference time-domain method and assessed against existing PhCs. Despite the design restrictions, we showed that a Q value up to 115,800 and Q/V values of 10^3–10^5 λ^{-3} are achievable without further design optimization. The results suggest that silicon (111) surfaces can be used for fabricating PhC nanocavity-based devices in a practical and economical way with high manufacturing tolerance and increased repeatability.

Contents

1. Introduction

With small footprints and low energy consumption reaching the order of fJ/bit, photonic crystals (PhCs) offer us a prospect of all-optical circuits, devices and interconnects in the future [1]. One remarkable feature of the PhC is its ability to confine light within nanocavities as an effect of both distributed Bragg reflection and internal reflection [2,3]. Nanocavities with ultra-high quality factors and extremely small mode volumes have been successfully applied to both active and passive devices, such as lasers [4–6], light-emitting diodes (LEDs) [7,8] and switches [9,10], transforming PhCs into essential building blocks for future optical devices.

PhCs are compatible with existing Complementary-Metal-Oxide-Semiconductor (CMOS) fabrication processes, but they are very sensitive to structural disturbances caused by line-edge roughness [11–13]. The conventional PhC slab is a triangular lattice of air holes in a dielectric slab and it remains a huge challenge to fabricate them with the very high accuracy of the order between 1 and 10 nm in a repeatable way [14]. Standard optical lithography processes, such as ArF and electron-beam, are known to cause roughness on the sidewalls, even for large feature sizes [15–17]. The minimum feature size of PhCs can be below 100 nm and structural disturbances in the atomic scale can have a detrimental effect on their performance, since scattering loss scales proportionally to $(\Delta n)^3$, where Δn is the difference of refractive indices between the slab and the cladding [12,18–20]. The ability to eliminate line-edge roughness would not only minimize scattering losses and improve the performance of the PhC, but also increase the fabrication tolerance, hence the repeatability and reliability of its production, by suppressing contribution to the standard deviation of the patterning position, which current conventional fabrication processes cannot guarantee yet.

* Corresponding author.
E-mail address: S.Saito@soton.ac.uk (S. Saito).

http://dx.doi.org/10.1016/j.photonics.2017.02.005

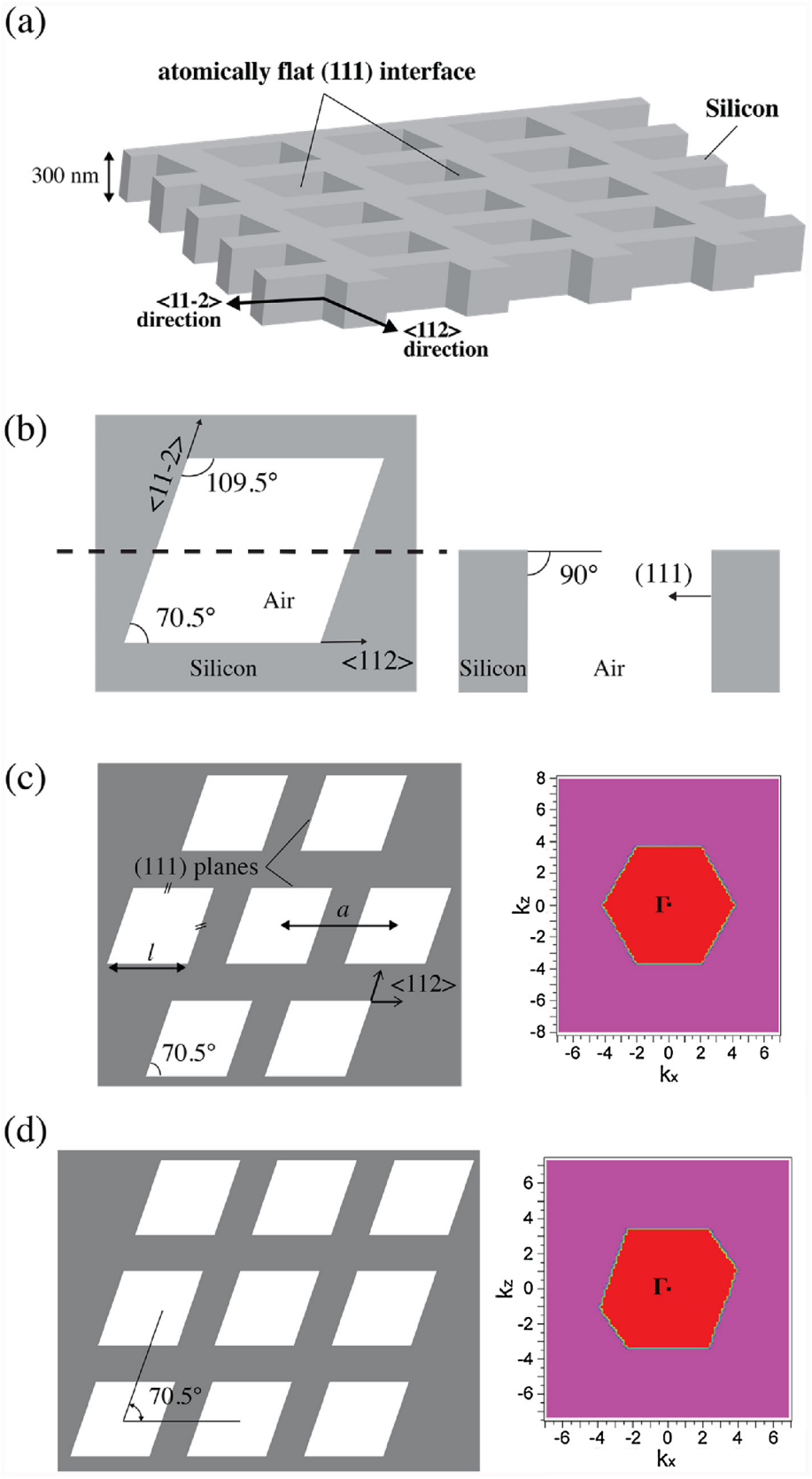

Fig. 1. (a) Schematic of 2-dimensional PhC silicon membrane with lattice points formed by Si (111) interfaces. (b) Cross-section of a parallelogram lattice point formed by Si (111) interfaces. (c) Triangular lattice configuration with parallelogram lattice points and its Brillouin zone. (d) Tilted square lattice configuration with parallelogram lattice points its Brillouin zone. k*x* and k*z* in the Brillouin zone are wave vectors in the reciprocal space in the *x*- and *z*-direction respectively.

One of the effective ways to reduce line-edge roughness is to use the anisotropic alkali wet etching technique [21]. Using an aqueous solution of tetramethylammonium hydroxide (TMAH) allows us to produce atomically flat silicon (Si) (111) interfaces due to the huge anisotropy of the etching rate against crystallographic orientations. The process is completely chemical, self-limited, compatible with existing patterning technologies [22,23], offering an economical alternative to the dry etching process with an extended manufacturing tolerance. This process already succeeds to produce highly reliable and easily passivated solar cells with pyramidal texture on wafer scale [24]. The rate of anisotropic wet etching is slow and solely determined by the crystal structure, but in turn it provides more precise control over the fabrication of sub-microns patterned structures. In fact, we have previously demonstrated slot waveguides and grating couplers using Si (111) interfaces fabricated at the Southampton Nanofabrication Centre, which show significant reduction in propagation losses. We used a custom-made Silicon-On-Insulator (SOI) substrate with Si (110) surface, on which Si (111) interfaces were defined perpendicular to the substrate along the <112> direction. For standard waveguides, this caused a reduction of propagation loss from 4.69 dB/cm (by dry etching) to 0.85 dB/cm in the TE mode, while for a slot waveguide it improved from 10.5 dB/cm to just 3.7 dB/cm [25,26].

Considering the advantages of this fabrication technique, we extended the idea of using the SOI wafer and atomically flat Si (111) surfaces for PhC-based cavities. Although Si (111) interfaces can produce cavity walls with reduced roughness, its use imposes strict limits on the design of the PhC, as only patterns shaped along <112> direction can be formed. In this work, we explored the feasibility of Si (111) interfaces for PhCs by simulating H1-, H0-, and L3-type nanocavities [26], which were optimized to achieve the fundamental TE mode at telecommunication wavelengths ($\lambda_c \approx 1550$ nm). Without further optimization to reduce leaky components of the confined mode, we observed the quality factor Q and the modal volume V, and used the ratio Q/V, which is proportional to the Purcell factor [28], to quantify the strength of the optical confinement. Furthermore, we compared the results with conventional PhCs that use circular holes and discovered that nanocavities with Si (111) interfaces show potential in strong optical confinement in spite of the design restrictions. The results suggest that anisotropic wet etching can establish a manufacturing process for PhCs without the requirement of costly, high accuracy equipment.

2. Photonic crystal design

We assumed the use of an SOI substrate with a 300 nm thick Si (110) layer and constructed PhC structures in a freestanding membrane with air holes (Fig. 1). The use of Si (111) interfaces significantly limits our freedom of design, because vertical Si (111) interfaces can only be formed along the <112> and <11-2> directions on the surface of the SOI layer, as shown in Fig. 1(b). As we were restricted to using only these two interfaces, the lattice point of our PhC becomes a parallelogram with interior angles of 70.53° and 109.47°. The trade-off between line edge roughness and freedom of design is interesting and the effects of this design restriction on the PhC's performance is worth investigating before proceeding to fabrication. We created a PhC with the triangular lattice using these parallelograms (Fig. 1(c)). For simplicity, we considered the sides of the parallelogram to be equal. Considering the unique symmetrical properties of the parallelogram pattern, we also designed an additional lattice, where we tilted a square lattice by 70.53° so that the symmetry of the whole lattice becomes the same as that of the lattice point (Fig. 1(d)).

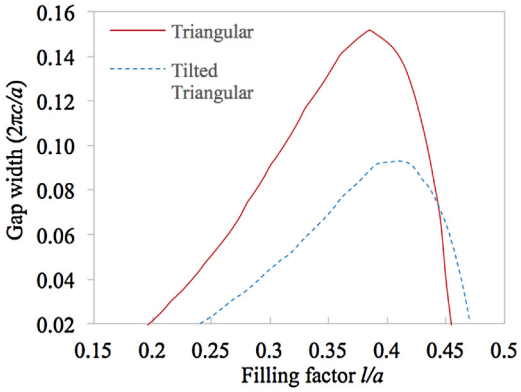

Fig. 2. Comparison of largest gap widths against filling fraction l/a between the triangular and tilted square lattice of PhCs formed by Si (111) interfaces.

We simulated the band structures for our novel PhC designs using the plane wave expansion method on the commercial software RSoft BandSOLVE and estimated the largest photonic band gap between the first and the second TE bands (Fig. 2) for various filling fractions defined as the ratio l/a, where l is the length of the side of the parallelogram and a is the lattice period. A large band gap should theoretically lead to a stronger optical confinement, as the range of frequency forbidden to the localized mode is extended, assuming that the mode is localized in the center of the gap [29]. Fig. 2 shows that the largest band gaps open when l/a is approximately 0.39 for the triangular lattice and 0.41 for the tilted square lattice. The band gaps of the tilted square lattice are always significantly narrower than that of the triangular lattice. Perhaps, the broken 6-fold rotational symmetry in the Brillouin zone (Fig. 1(d)) has reduced the band gaps size, due to the belonging of the pattern to a lower symmetry group than the unit cell [30]. Even so, the filling fractions maximizing the band gaps served as a starting point to design the high-Q nanocavity structures.

3. Nanocavity simulations

In order to investigate the optical confinement capability, we introduced H1-, H0- and L3-type cavities into the triangular and tilted square lattices (Fig. 3). To ensure a well-confined mode, a 17×17 lattice periods structure was used. We simulated the cavities as a 300 nm thick freestanding silicon membrane ($n = 3.477$)

Table 1
Cavity characteristics for each lattice configuration.

	H1 Triangular		H1 Tilted Square		H0 Triangular		H0 Tilted Square		L3 Triangular	
Lattice point	Circular	Si (111)	Circular	Si (111)	Circular	Si (111)	Circular	Si (111)	Circular	Si (111)
a (nm)	0.402	0.383	0.421	0.412	0.422	0.412	0.442	0.385	0.377	0.390
Ratio l/a	0.484	0.370	0.300	0.510	0.510	0.424	0.620	0.480	0.490	0.500
d (nm)	–	–	–	–	0.15a	0.15a	0.17a	0.27a	0.20a	0.15a
λ_c (nm)	1552.2	1552.6	1549.6	1548.9	1550.0	1555.4	1581.2	1547.8	1575.0	1563.1
Q	609	1646	344	377	193,286	115,786	10,801	2245	168,767	59,400
$V\,(\lambda/n)^3$	0.239	0.600	0.535	0.498	0.215	0.478	0.512	0.649	0.831	1.861
$Q/V\,(\lambda^{-3})$	2548	2743	643	757	899,005	242,230	21,096	3459	203,179	31,923

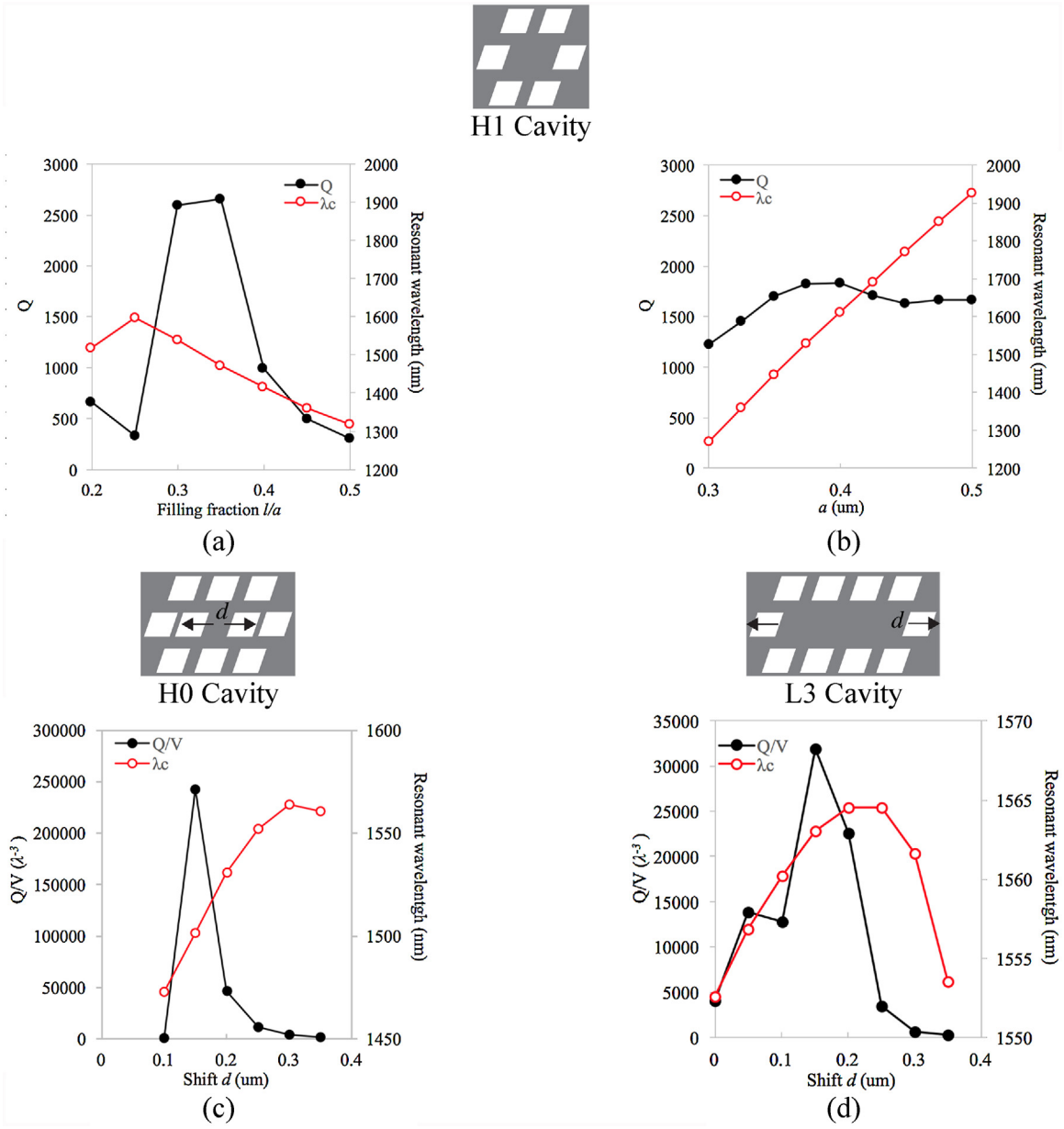

Fig. 3. Optimization of the quality factors in Si (111)-based photonic crystals. (a) Dependence of the filling fractions on resonant wavelengths and Q in the H1 cavity in the triangular lattice. (b) Dependence of lattice period a at a fixed filling fraction of $l/a = 0.37$ on the resonant wavelengths and Q in the H1 cavity in the triangular lattice. (c) Optimization of the shift distance d in the H0 cavity in the triangular lattice. (d) Optimization of the shift distance d in the L3 cavity.

and used the three-dimensional finite-difference time-domain (3D-FDTD) method [31] on the commercial software Lumerical to calculate Q and V of the fundamental TE cavity mode. Perfectly matched layers (PML) absorbing conditions were used at the boundaries, but due to the unique symmetrical features of the structures, we could not make use of symmetric boundary conditions in the x- and y-directions to reduce the computing time. We found that applying a magnetic dipole source operating at a range of 1400–1700 nm isolates the resonant peak of the lowest energy mode λ_c at 1550 nm.

The results are summarized in Table 1. The H1 cavity was formed by removing one lattice point in the center of the PhC [32], while the H0 cavity was formed by shifting two adjacent holes in the center of the PhCs oppositely along the x-direction by a distance d [27]. The L3 cavity was formed after removing three adjacent lattice points in the center, while the holes at the edges of the cavity were shifted by d in order to reduce the leaky components responsible for radiation losses as much as possible and thus strenghten the optical confinement [33]. Our design objective was to make PhC cavities with λ_c close to 1550 nm. First, we changed the l/a ratio to yield the highest Q value regardless of λ_c. Then we set the l/a ratio to the optimum value and changed a to obtain a λ_c close to 1550 nm. We observed that an increase of a leads to a redshift of λ_c (Fig. 3(b)), while an increase of l/a leads to a blueshift (Fig. 3(a)), suggesting the scalability of the design for operations at various wavelengths. This design process was iterative; we started with estimating optimum values of l/a and a based on the band gap simulations, then optimized the two parameters repeatedly as we approached the desired λ_c with a reasonably high Q value.

H0 and L3 cavities have an additional parameter d to tune the condition for the confinement. In the case of H0, the optimization of d was made before scanning for the other two parameters, as it is d that creates the space to confine light [27]. On the other hand, in the L3 cavity, d defines the confined field envelope in the cav-

Table 2
Field profiles of each cavity and lattice configuration (For interpretation of the references to colour in this table legend, the reader is referred to the web version of this article).

	Circular Lattice Point	Si (111) Lattice Point
H1 Triangular	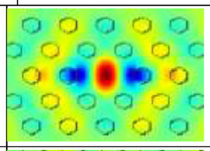	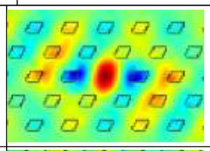
H1 Tilted Square	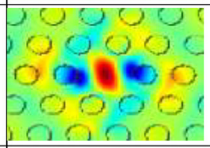	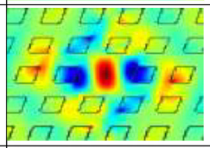
H0 Triangular	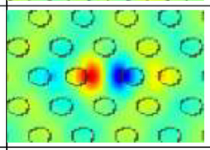	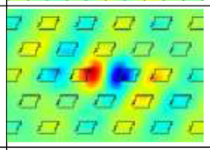
H0 Tilted Square	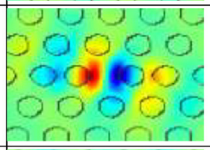	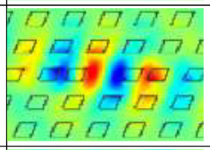
L3 Triangular	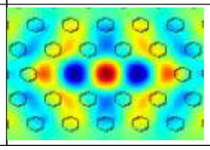	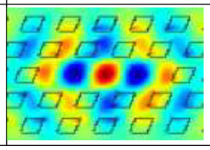

ity without a significant shift of the confined wavelength. In other words, this spatial change redistributes the field components in the momentum space (k-space) after the Fourier transform and the right amount lightens the field components inside the light cone ($k < 2\pi/\lambda$) liable for out-of-plane radiation losses, enhancing the photon lifetime inside the cavity [33]. Hence, the optimization of d for L3 was made after the optimization of l/a and a. For both cavities, we observed that there is an optimum d for an ideal confinement, but a larger shift leads to a leak (Fig. 3(c) and 3(d)). While λ_c scales proportionally with a and l/a, there is a maximum λ_c against d in the H0 and L3 cavities (Fig. 3(c) and (d)). After the determination of the structural parameters, we calculated V. The L3 cavity of the tilted square lattice, was not able to carry a unique radiation intensity pattern; an electric dipole moment, due to the surrounding photonic crystal structures inhibiting the slackness of such modes within such cavity size (~1.2 μm). Higher order modes in L3 lattices can still be useful, as demonstrated for pumping in low threshold nanocavity lasers [34]. In this work, we were mainly concerned about the fundamental mode, so that this cavity was not included in the results in Table 1. Ultimately, for comparison, we simulated conventional PhCs with circular holes for each type of cavity and lattice configuration that we considered following the same optimization process as our Si (111) structures.

From the field distributions shown in Table 2, we found that the parallelogram-shaped cavities cause losses in optical confinement when compared to the circular cavities. Compared to air holes in a hole slab, the slanted sides of the parallelogram pattern break the mirror symmetries of the mode along the x and y-axis but preserve the 2-fold axis symmetry, slightly tilting the shape of the mode to the right following the shape of the cavity. Due to the particular pattern and the field penetration in the lower index regions caused by the sharp edges, V of PhCs with parallelogram lattice are two to three times larger than the conventional PhCs. Such larger V would affect the spontaneous emission rate of an emitter inside the cavity and would not be ideal for increasing the integration density of optical devices [35]. Even so, this concentration of the field in lower index region can be interesting with a cladding other than air, such as Electro-Optic Polymer (EOP) [36], allowing dynamic control of the resonant wavelength of the cavity for applications such as Quantum Information Processing.

In terms of the strengths of the confinements, the H1 cavity exhibited a Q/V value comparable with conventional PhCs – a higher Q value, but also a significantly larger V, which counterbalances the confinement strength (Table 1). The tilted square lattice also yielded Q and V values similar to the conventional PhC, but when compared to the triangular lattice, the Q/V was lower. This was expected, as the band gaps of tilted square lattices were observed to be narrower than that of triangular lattices (Fig. 2). The H0 and L3 cavities of the Si (111) structures showed significant differences in Q/V from the conventional PhCs. A shift of $d = 0.15a$ in the L3 cavity yielded a Q value of 59,400 and consequently led to an 8-fold improvement in Q/V from approximately 4000 to 32,000 (Fig. 3(d)). In spite of that, this Q/V value is still an order of magnitude less than that of the conventional PhC, which is attributable to its huge V reaching to 1.9 $(\lambda/n)^3$. The highest Q value of 115,800 was achieved by the H0 cavity with a shift of $d = 0.15a$. Although the Q value seems comparable with the conventional PhC, its V is more than twice larger, reducing the Q/V value of the Si (111) PhC to just 242,000. Even so, this is the highest Q/V value among all Si (111) structures.

The lower Q values in Si (111) cavities would be due to the abrupt edges of the parallelogram-shaped cavity. In-plane confinement within a PhC is achieved by spatial localization, adding up partial reflections of light at the edges of the cavity. The electric field profile inside a cavity can be expressed by an envelope function $F(x)$ multiplied by the sinusoidal light wave of wavelength λ. To achieve strong confinement and a high Q, the key condition is to satisfy a Bragg reflection that can produce a gentle electric field

envelope profile inside the cavity, such as a Gaussian envelope [33]. In the case of a conventional PhC with circular holes, light tends to be reflected off the edges in a continuous manner, supporting the formation of a perfect Gaussian curve within the cavity. Any irregularity at the cavity's edges would affect the partial reflection paths, modifying the envelope function, hence causing out of plane radiation losses. In the case of our PhCs with parallelogram-shaped pattern, the envelope function is not as smooth as the cavities with circular holes can be. This is due to the slanted sides and the sharp edges of the parallelogram patterns reducing the symmetry regardless the lattice on the contrary of the air holes having cylindrical symmetry, involving the electric field to be reflected at dielectric/air interfaces with more varying non-matching phases and directions. As a consequence of the non-parallel symmetry axis of the mode in the cavity, a perfect Gaussian-shaped field profile was not possible to form. In the case of the H1 cavity, the positioning of its six neighboring lattice points in the triangular lattice is still able to reduce out-of-plane radiations quite well, which can be seen from the high Q value that is even higher than the conventional PhC, but the asymmetrical shape of the cavity itself fails to supply a sufficiently gentle field profile for a perfect a Gaussian field, leading to a large V that eventually pulls down the Q/V value. Although the tilted square lattice has a cavity shape with more symmetry, we suspect that the small band gap produced by the lattice and was the cause of the lower Q/V value.

It was more difficult to achieve perfect confinement conditions within the H0 and L3 cavities than in the H1 cavity. Shifting the holes at the edges of the L3 cavity increased Q, which is in agreement with the findings of Akahane et al. However, we believe that the slanted sides of the pattern could not support a sufficiently gentle confinement to maximize the Q values despite the shift. A similar argument applies for H0, where the confinement was mainly observed between the two slanted sides of the edges. As seen in Table 2, the two mode maxima inside the cavity are more dispersed along the slanted edges. The H0 cavity is known for being able to achieve ultra-small V, but existing studies have included optimizations to the air holes around the cavity, which enabled them to achieve an ultra-high Q while maintaining the very small V [27,37,38]. Among all Si (111) structures, the H0 cavity in the triangular lattice indeed produced the smallest V of 0.48 $(\lambda/n)^3$, but even that is still more than double than the conventional PhC. Further optimizations to the dimensions of the air holes, such as position and size, may increase the Q of the H0 cavity in the Si (111) structure, but the field profile may stay dispersed along the edges due to the reflection conditions imposed by the slanted sides, keeping the modal volume large. Regardless of these disadvantages, we have managed to achieve a Q/V value in the order of 10^4-10^5 λ^{-3} for both L3 and H0 cavities. Without further structural optimizations, the current design can already be useful for some applications in devices only requiring moderate Q-factors ($\sim 10^5$), such as optical sensors [39,40], and optical switches with fast response times [1,41].

4. Conclusion

We have theoretically examined the impacts of Si (111) interfaces on the optical confinement of PhC nanocavities. The simulations showed that in spite of the design restrictions posed by the Si (111) surfaces, these nanocavities can still realize strong confinements. We have demonstrated that Q values up to 115,800 and Q/V values in the range of 10^3–10^5 λ^{-3} are achievable. Due to the unique shape of the pattern, the confined mode is leaky and the modal volumes are relatively large. Losses were observed due to the abrupt field profile inside the cavity. Despite that, we believe that the Q values can still be increased by further optimizations of the lattice points position around the cavities. Fabrication of the structures will take into account the reduced line edge roughness by the wet etching technique and we expect even further performance improvements. All in all, we showed that Si (111) interfaces offer a method of producing nanocavities with potentially strong confinement capabilities, while expanding the manufacturing tolerance and increasing the repeatability of the whole process.

Acknowledgements

This work is supported by EPSRC Standard Grant (EP/M009416/1), EPSRC Manufacturing Fellowship (EP/M008975/1), EPSRC Platform Grant (EP/N013247/1), and EU FP7 Marie-Curie Carrier-Integration-Grant (PCIG13-GA-2013-618116). The data from the paper can be obtained from the University of Southampton ePrint research repository: http://eprints.soton.ac.uk/401306/

References

[1] M. Notomi, Manipulating light with strongly modulated photonic crystals, Reports Prog. Phys. 73 (9) (2010) 96501.
[2] S. John, Strong localization of photons in certain disordered dielectric superlattices, Phys. Rev. Lett. 58 (no. 23) (1987) 2486–2489.
[3] J. Vučković, M. Lončar, H. Mabuchi, A. Scherer, Design of photonic crystal microcavities for cavity QED, Phys. Rev. E 65 (1) (2001) 16608.
[4] M. Lončar, T. Yoshie, A. Scherer, P. Gogna, Y. Qiu, Low-threshold photonic crystal laser, Appl. Phys. Lett. 81 (15) (2002) 2680.
[5] S. Noda, Photonic crystal lasers—ultimate nanolasers and broad-area coherent lasers [Invited], J. Opt. Soc. Am. B 27 (11) (2010) B1–B8.
[6] K. Hirose, Y. Liang, Y. Kurosaka, A. Watanabe, T. Sugiyama, S. Noda, Watt-class high-power, high-beam-quality photonic-crystal lasers, Nat. Photonics 8 (5) (2014) 406–411.
[7] C. Wiesmann, K. Bergenek, N. Linder, U.T. Schwarz, Photonic crystal LEDs—designing light extraction, Laser Photon. Rev. 3 (3) (2009) 262–286.
[8] J.J. Wierer, A. David, M.M. Megens, III-nitride photonic-crystal light-emitting diodes with high extraction efficiency, Nat. Photonics 3 (3) (2009) 163–169.
[9] M. Belotti, J.F. Galisteo-López, S. De Angelis, M. Galli, I. Maksymov, L.C. Andreani, D. Peyrade, Y. Chen, All-optical switching in 2D silicon photonic crystals with low loss waveguides and optical cavities, Opt. Express 16 (15) (2008) 11624–11636.
[10] K. Nozaki, E. Kuramochi, A. Shinya, M. Notomi, 25-channel all-optical gate switches realized by integrating silicon photonic crystal nanocavities, Opt. Express 22 (12) (2014) 14263–14274.
[11] Z.H. Zhu, W.M. Ye, J.R. Ji, X.D. Yuan, C. Zen, Influence of random errors on the characteristics of typical 2D photonic crystal microcavity, Appl. Phys. B Lasers Opt. 88 (2007) 231–236.
[12] H. Hagino, Y. Takahashi, Y. Tanaka, T. Asano, S. Noda, Effects of fluctuation in air hole radii and positions on optical characteristics in photonic crystal heterostructure nanocavities, Phys. Rev. B, vol. 79 (8) (2009) 85112.
[13] W. Fan, Z. Hao, Z. Li, Y. Zhao, Y. Luo, Influence of fabrication error on the characteristics of a 2-D photonic-crystal cavity, J. Lightw. Technol. 28 (10) (2010) 1455–1458.
[14] W. Bogaerts, R. Baets, P. Dumon, V. Wiaux, S. Beckx, D. Taillaert, B. Luyssaert, J. Van Campenhout, P. Bienstman, D. Van Thourhout, Nanophotonic waveguides in silicon-on-Insulator fabricated with CMOS technology, J. Lightw. Technol. 23 (1) (2005) 401.
[15] K.K. Lee, D.R. Lim, H.C. Luan, A. Agarwal, J. Foresi, L.C. Kimerling, Effect of size and roughness on light transmission in a Si/SiO_2 waveguide: experiments and model, Appl. Phys. Lett. 77 (11) (2000) 1617.
[16] W. Bogaerts, P. Bienstman, R. Baets, Scattering at sidewall roughness in photonic crystal slabs, Opt. Lett. 28 (9) (2003) 689–691.
[17] C. Qiu, Z. Sheng, H. Li, W. Liu, L. Li, A. Pang, A. Wu, X. Wang, S. Zou, F. Gan, Fabrication, characterization and loss analysis of silicon nanowaveguides, J. Lightw. Technol. 32 (13) (2014) 2303–2307.
[18] S. Suzuki, M. Yanagisawa, Y. Hibino, K. Oda, High-density integrated planar lightwave circuits using SiO_2-GeO_2 waveguides with a high refractive index difference, J. Lightw. Technol. 12 (5) (1994) 790–796.
[19] R.A. Lawson, C.L. Henderson, Understanding the relationship between true and measured resist feature critical dimension and line edge roughness using a detailed scanning electron microscopy simulator, J. Vac. Sci. Technol. B 28 (6) (2010) C6H34.
[20] C. Shin, Line Edge Roughness (LER), in Variation-Aware Advanced CMOS Devices and SRAM, 1st ed., Springer, Dordrecht, Netherlands, 2016, pp. 19–35.
[21] K.K. Lee, D.R. Lim, L.C. Kimerling, J. Shin, F. Cerrina, Fabrication of ultralow-loss Si/SiO_2 waveguides by roughness reduction, Opt. Lett. 26 (23) (2001) 1888–1890.
[22] C.H. Han, E.S. Kim, Study of self-limiting etching behavior in wet isotropic etching of silicon, Jpn. J. Appl. Phys. 37 (12S) (1998) 6939.

[23] R.E. Oosterbroek, J.W. Berenschot, H.V. Jansen, A.J. Nijdam, G. Pandraud, A. van den Berg, M.C. Elwenspoek, Etching methodologies in <111>-oriented silicon wafers, J. Microelectromech. Syst. 9 (3) (2000) 390–398.
[24] P. Papet, O. Nichiporuk, A. Kaminski, Y. Rozier, J. Kraiem, J.F. Lelievre, A. Chaumartin, A. Fave, M. Lemiti, Pyramidal texturing of silicon solar cell with TMAH chemical anisotropic etching, Sol. Energy Mater. Sol. Cells 90 (15) (2006) 2319–2328.
[25] K. Debnath, H. Arimoto, M.K. Husain, A. Prasmusinto, A. Al-Attili, R. Petra, H.M.H. Chong, G.T. Reed, S. Saito, Low-loss silicon waveguides and grating couplers fabricated using anisotropic wet etching technique, Front. Mater. 3 (10) (2016) 1–7.
[26] K. Debnath, A.Z. Khokhar, S.A. Boden, H. Arimoto, S.Z. Oo, H.M.H. Chong, G.T. Reed, S. Saito, Low-loss slot waveguides with silicon (111) surfaces realized using anisotropic wet etching, Front. Mater. 3 (51) (2016) 1–5.
[27] Z. Zhang, M. Qiu, Small-volume waveguide-section high Q microcavities in 2D photonic crystal slabs, Opt. Express 12 (17) (2004) 3988–3995.
[28] E.M. Purcell, Spontaneous emission probabilities at radio frequencies, Phys. Rev. 69 (1946) 681.
[29] J.D. Joannopoulos, S.G. Johnson, J.N. Winn, R.D. Meade, The Multilayer Film: A One-Dimensional Photonic Crystal, in Photonic Crystals: Molding the Flow of Light, 2nd ed., Princeton Univ. Press, 2008, pp. 44–65.
[30] R. Wang, X.-H. Wang, B.Y. Gu, G.Z. Yang, Effects of shapes and orientations of scatterers and lattice symmetries on the photonic band gap in two-dimensional photonic crystals, J. Appl. Phys. 90 (9) (2001) 4307.
[31] K. Yee, Numerical solution of initial boundary value problems involving maxwell's equations in isotropic media, IEEE Trans. Antennas Propag. (1966) 302–307.
[32] O. Painter, J. Vučković, A. Scherer, Defect modes of a two-dimensional photonic crystal in an optically thin dielectric slab, J. Opt. Soc. Am. B 16 (2) (1999) 275–285.
[33] Y. Akahane, T. Asano, B.-S. Song, S. Noda, High-Q photonic nanocavity in a two-dimensional photonic crystal, Nature 425 (6961) (2003) 944–947.
[34] M. Nomura, S. Iwamoto, M. Nishioka, S. Ishida, Y. Arakawa, Highly efficient optical pumping of photonic crystal nanocavity lasers using cavity resonant excitation, Appl. Phys. Lett. 89 (16) (2006) 161111.
[35] R. Coccioli, M. Boroditsky, K.W. Kim, Y. Rahmat-Samii, E. Yablonovitch, Smallest possible electromagnetic mode volume in a dielectric cavity, Proc. IEEOptoelectron. 145 (6) (1998) 391–397.
[36] M. Nakadai, R. Konoike, Y. Tanaka, T. Asano, S. Noda, Design of double-slotted high-Q photonic crystal nanocavity filled with electro-optic polymer, in: OptoElectronics and Communications Conference (OECC) Held Jointly with 2016 International Conference on Photonics in Switching (PS), IEEE, 2016, pp. 1–3 (21st).
[37] M. Nomura, K. Tanabe, S. Iwamoto, Y. Arakawa, High-Q design of semiconductor-based ultrasmall photonic crystal nanocavity, Opt. Express 18 (8) (2010) 8144–8150.
[38] U.P. Dharanipathy, M. Minkov, M. Tonin, V. Savona, R. Houdré, High-Q silicon photonic crystal cavity for enhanced optical nonlinearities, Appl. Phys. Lett. 105 (September (10)) (2014) 101101.
[39] Y. Liu, H.W.M. Salemink, Photonic crystal-based all-optical on-chip sensor, Opt. Express 20 (18) (2012) 19912–19920.
[40] Y. Zhang, Y. Zhao, R. Lv, A review for optical sensors based on photonic crystal cavities, Sens. Actuators A 233 (2015) 374–389.
[41] T. Tanabe, H. Taniyama, M. Notomi, Carrier diffusion and recombination in photonic crystal nanocavity optical switches, J. Lightw. Technol. 26 (11) (2008) 1396–1403.